Available online at www.sciencedirect.com
ScienceDirect
Journal of Power Sources 160 (2006) 1495–1500
JOURNAL OF POWER SOURCES
www.elsevier.com/locate/jpowsour

Short communication

Effects of microporosity on the specific capacitance of polyacrylonitrile-based activated carbon fiber

Jong-Gyu Lee [a], Je-Young Kim [a], Sung-Hyun Kim [b,*]

[a] *Energy Res. Team, Research Institute of Science and Technology (RIST), Pohang, Republic of Korea*
[b] *Department of Chemical & Biological Eng., Korea University, Seoul, Republic of Korea*

Received 25 November 2005; received in revised form 5 February 2006; accepted 6 February 2006
Available online 29 March 2006

Abstract

Polyacrylonitrile (PAN)-based, microporous activated carbon fibers (ACFs) were investigated as electrode materials for electrochemical capacitors in KOH electrolyte solutions. PAN–ACFs were analyzed by using nitrogen adsorption data and the Dubinin–Raduskevich equation. The pore size distributions were narrow. As the micropore volume increased, the average micropore diameter decreased. Cyclic voltammetry (CV), electrochemical impedance spectroscopy (EIS) and charge–discharge profile analysis were used to investigate the penetrability of electrolyte ions into the carbon electrodes. The electrolyte ions in the carbon electrode with a large micropore diameter could be accessible easily even if the pore size distribution is narrow. However, the specific capacitance decreased in spite of the increase of the micropore volume.

Keywords: PAN–ACF; Tension; Micropore; Specific capacitance; Impedance spectroscopy

1. Introduction

Porous carbon is used as an electrode material in double-layer capacitors (EDLCs) because of its large specific surface area, high electricalconductivity, structural stability, and environmental compatibility [1–4]. The electrochemical characteristics of EDLCs with carbon electrodes rely heavily on the material properties of the carbon such as its specific surface area (SSA), pore size distribution, shape of pores, and surface functional groups including its purity and electrical conductivity [5–11]. In general, a higher specific capacitance is known to be obtained with a higher SSA of the carbon. Still, higher SSA does not guarantee a higher specific capacitance particularly at high SSA, i.e., the ions of electrolytes cannot access all of the pores of porous carbon. Recently, carbon fibers with a high surface area and fiber-derived products such as cloth have been gaining increased attention for use in EDLCs [12–15]. The use of carbon fibers has several distinct advantages over the particle-based approach; in particular, the pore size and structure of the electrode are readily controlled and tailored to a specific application by varying both the diameter and length of carbon fibers. The access of the ions of the electrolytes is expected to play an important role in microporous carbon materials [16–19].

In this study, the microporosity of polyacrylonitrile-based activated carbon fiber(PAN–ACF) was controlled by applying the tension during the stabilization of PAN fiber and changing the KOH/carbon ratio for the fibers with the constant tension. Porous activated carbon fibers with varying microporosity were used as electrode materials for EDLCs. Finally, the electrochemical characteristics were evaluated.

2. Experimental

2.1. Preparation of PAN–ACF

PAN precursor fiber (copolymer, Courtaulds Company) tows containing 12,000 1.12-denier filaments were used as starting materials. The stabilized fiber was prepared at 250 °C for 3 h in a forced convection oven. In preparing the stabilized fiber, tension was applied to tows with one end of the fiber fixed; a constant weight was hung at the other end. The stabilized fiber without the tension was labeled as T01. The stabilized fiber applying a tension of 600 g_f was labeled as T61. The fibers were

* Corresponding author. Tel.: +82 2 3290 3297; fax: +82 2 926 6102.
E-mail address: kimsh@korea.ac.kr (S.-H. Kim).

0378-7753/$ – see front matter © 2006 Elsevier B.V. All rights reserved.
doi:10.1016/j.jpowsour.2006.02.016

immersed in a 1-mole KOH solution for 1 h and then filtered and dried. The stabilized fibers stained with KOH were crushed using a mixer mill (Retsch M350, Germany). In particular, the stabilized fiber subjected to a tension of 600 g_f was impregnated with a 3-mole KOH solution for 1 h. This sample was labeled as T63. The crushed fibers were heat-treated at 800 °C under a nitrogen atmosphere for 1 h and then washed using diluted 0.5 N hydrochloric acid and hot water and finally dried. ACFs were screened by length (38 μm or less).

2.2. Carbon characterization

Nitrogen adsorption isotherms were measured at 77 K using ASAP 2010 (Micromeritics). Prior to each measurement, samples were degassed at 573 K for 10 h. The specific surface area of the sample was calculated using the BET model and the micropore volumes were determined from Dubinin–Radushkevich (DR) equations. Pore size distribution was then calculated using the DFT program provided by Micromeritics.

2.3. Electrochemical measurements

Two-electrode capacitors were built from all of the ACFs. The electrode consisted of 85% ACF, 9% Super-P, 1% VGCF (Vapor Grown Carbon Fiber), and 5% binder (3% carboxymethyl cellulose, 2% styrene butadiene rubber). The electrolyte was a 6 M KOH aqueous solution, and all the electrodes used had an exposed area of 4 cm × 4 cm. The current collector used Ni foam electrode and Ni foil lead wire connection. For the electrochemical measurements, impedance spectroscopy (Solatron, IM6) was used with 5 mV excitation. Cyclic voltammetry (EG&G, Princeton Applied Model 273A) was performed in the double layer region of potential ranging from 0 to 0.9 V in 6M KOH electrolyte solution. All the electrochemical measurements were conducted at ambient temperature.

3. Results and discussion

3.1. Pore structure analysis

Fig. 1 shows the nitrogen adsorption/desorption isotherms of the samples at 77 K. The isotherms of all samples are typical of type I which proves the existence of a microporous structure. Generally, the isotherm shapes were similar for all samples. At high relative pressures, the T63 isotherm shows a hysteresis loop, which indicates that the sample contains some mesopores. The mesopores of T63 are negligible compared to the micropores.

The nitrogen isotherm of T63 also shows a remarkable uptake at relative pressure in the range of 0.01–0.2, which is ascribed to the presence of larger micropores. The adsorption in micropores occurs by a "cooperative pore filling" mechanism, which corresponds to the filling process by molecules on the monolayer-coated micropore walls [20].

Consequently, the second-layer adsorption occurs at rather low relative pressures, producing an initial uptake for T63, as shown in Fig. 1.

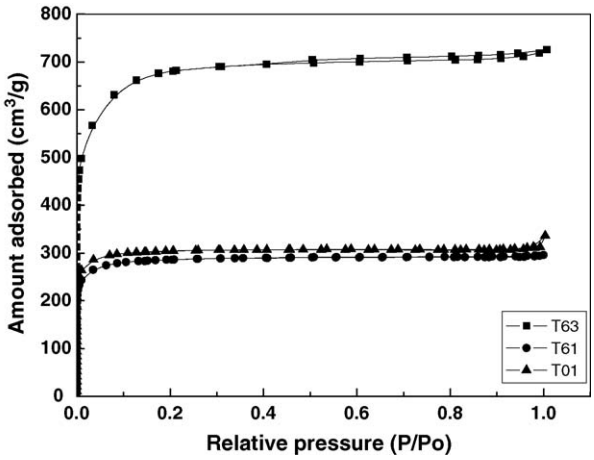

Fig. 1. Nitrogen adsorption isotherm.

As the low-pressure region of the adsorption isotherms is very important, it is preferable to express the pressure axis of the isotherm on a logarithmic scale. In order to analyze the shape of the nitrogen isotherms over the range of low relatively pressures, the experimental data are also presented in Fig. 2.

The marked adsorption of nitrogen below $P/P_0 = 10^{-5}$ is caused by the accelerated bilayer adsorption discussed above. The increase after the initial rapid uptake is due to the dominant cooperative pore filling of the residual space between the second adsorbed layers on the walls of slightly larger micropores.

It could be shown from Fig. 1 that the knee of T63 isotherm has a more rounded shape under $P/P_0 = 0.2$. In Fig. 2, the rapid adsorption occurred in the range of relative pressure between 10^{-5} and 10^{-1}.

As showed in Table 1, the increase of surface area causes an increase of the micropore volume for the carbon samples. When polyacrylonitrile fibers are heated in an oxidizing atmosphere under tension, the reorganized polymer chains align to form an oxygen-aided three-dimensional linkage of parallel molecular chains. This ladder formation reaction keeps the chains aligned parallel to the axis even after the release of tension following the treatment [21]. Some uncyclized structure left after stabilization due to tension, are removed in the form of volatile products dur-

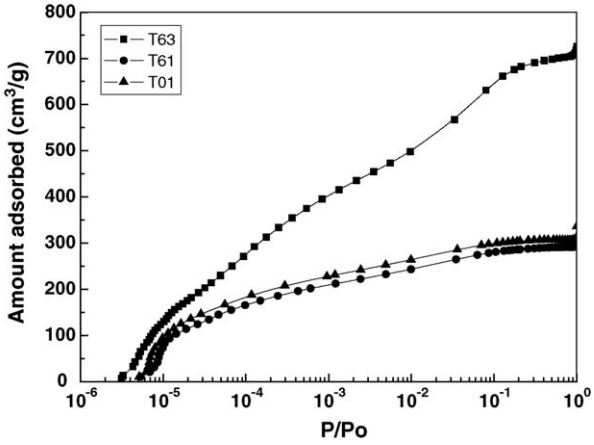

Fig. 2. Adsorption isotherms of the samples in the wide pressure range.

Table 1
Physical properties of the carbon samples

Carbon	S_{BET}[a] ($m^2\ g^{-1}$)	V_{mic}[b] ($cm^3\ g^{-1}$)	d[c] (Å)	E_0[d] ($kJ\ mol^{-1}$)	Capacitance[e] (Fg^{-1})
T01	1005	0.51	7.0	17.63	126
T61	935	0.48	7.1	17.55	142
T63	2312	1.23	6.3	18.77	113

[a] Surface area by BET model.
[b] Micropore volume by DR plot.
[c] Average micropore diameter by Stoeckli et al. [21].
[d] Characteristic energy by DR-plot.
[e] Specific capacitance by impedance spectroscopy.

ing a subsequent thermal process, and this leads to the formation of voids in the final structure of the carbon fibers. The surface area of T01 is larger than that of T61 owing to the uncyclized regions.

Stoeckli [22] proposed the following relation between the characteristic energy (E_0) and the average pore diameter (d).

$$d = \frac{30}{E_o} + \frac{5705}{E_o} + \frac{0.028}{E_o} - 1.49$$

in which d is the average micropore diameter expressed in nm and E_0 is given in $kJ\ mol^{-1}$.

This equation means that the larger the characteristic energy (E_0) the smaller the micropore diameter [23,24].

Fig. 3 shows the pore size distribution of all carbon samples. From the pore size distribution shapes in Fig. 3 one could conclude that all the studied carbons possess narrow pores; however, major contribution to the porosity is given by pores at pore diameter >7 Å. The pore size distribution of T63 becomes narrower although it contains the larger micropore sizes.

This pore narrowing is associated with the structural rearrangements of the crystallites and also with the shrinkage of the fiber, which occurs during the thermal treatment. Upon treating the samples by means of KOH activation, the pore network would be developed through deeper insertion of potassium attached to the fiber. The activation process broadens first the interstices between the structural units, and further reaction causes to destroy overall fiber structure to be rearranged into accumulative amorphous carbons [25,26].

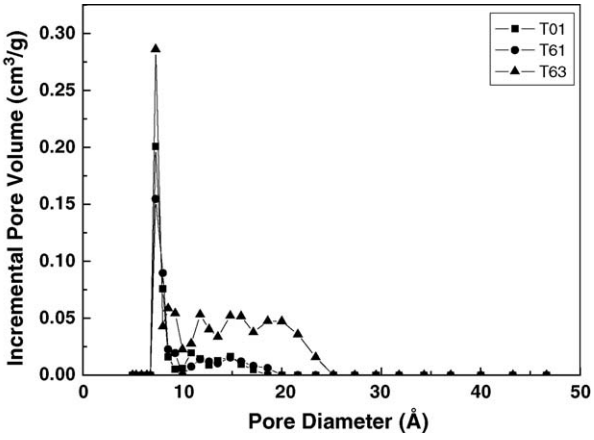

Fig. 3. Pore size distributions of the samples by density functional theory (DFT).

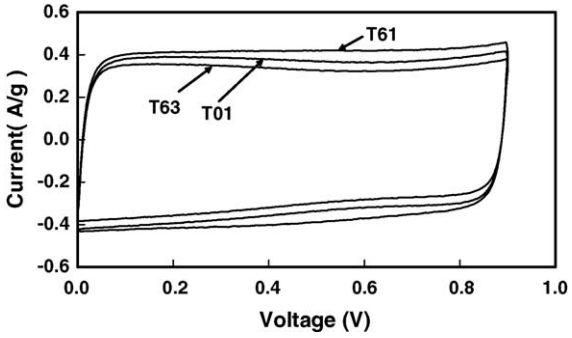

Fig. 4. Cyclic voltammograms of the porous carbon electrode.

3.2. Electrochemical characteristics

Fig. 4 shows the cyclic voltammograms experimentally obtained from the carbon electrode in a 6M KOH electrolyte solution at sweep rate of $10\ mV\ s^{-1}$. The voltammograms were recorded in the potential range between 0 and 0.9 V. No visible peaks due to redox reactions were observed at the applied potential sweep rate. At a voltage sweep rate of $10\ mV\ s^{-1}$, the carbon electrodes show the rectangular shape indicative of capacitive behavior. However, the rectangular shape of T61 is less distorted than that of T63, which indicates a good capacitive behavior. Generally, the accessibility of the ions onto the electrochemically active surface depends upon the pore diameter of the active materials. The accessibility of ions to the T61 sample could be better than that of T63 due to the larger pore diameter in spite of the fact that the surface area of T63 is large. These results agree with Fig. 5.

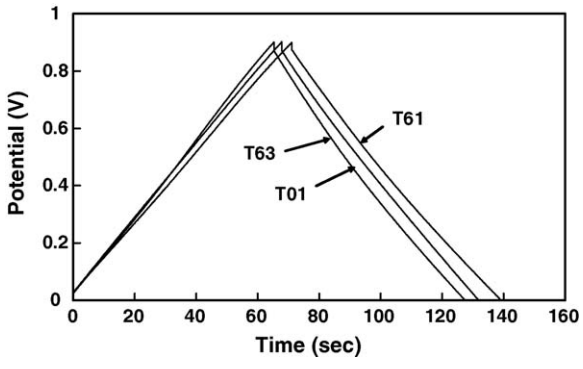

Fig. 5. Charge/discharge characteristics of the carbon electrode.

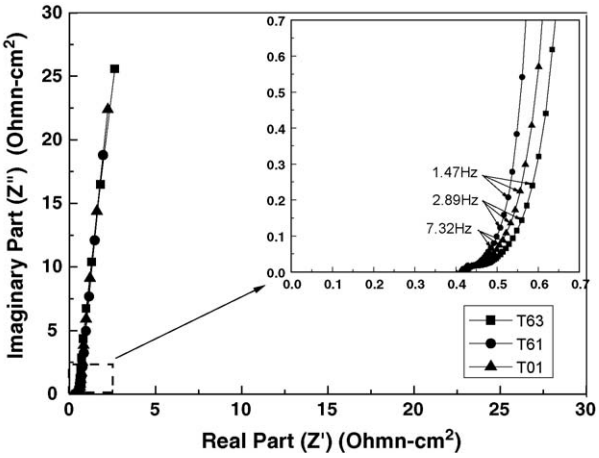

Fig. 6. Nyquist plots of ac impedance measurements.

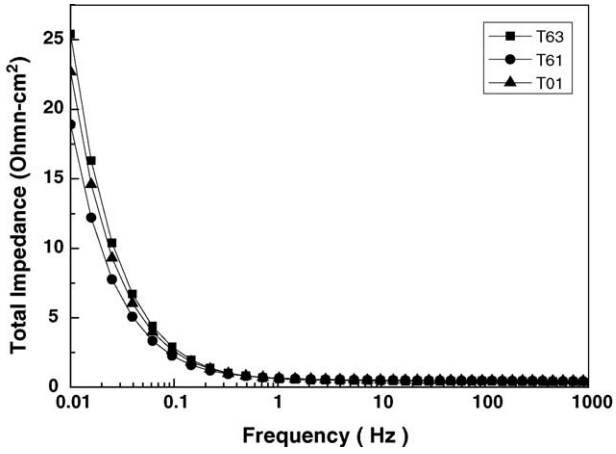

Fig. 7. Total impedance vs. frequency plot by impedance spectroscopy.

Fig. 5 exhibits charge–discharge curves (at the tenth cycle) for the carbon electrodes using a 6 M KOH aqueous solution at 10 mA cm^{-2}. The curves were nearly linear, indicating that a good electrode/electrolyte interface was accomplished. The carbon electrode displays a typical charge–discharge performance with a very low ohmic resistance at the potential switching point.

The Nyquist plots are shown for 4 cm × 4 cm cells assembled with two electrodes in Fig. 6. The frequency range studied is 0.01 Hz–10 MHz. The intersect in Fig. 6 shows the high frequency range. Fig. 6 shows that the carbon electrode behaves as a pure resistor at high frequencies and as a capacitor at low frequencies. In the mid frequency range, it behaves as a combination of resistor and capacitor, where the electrode porosity and pore shape of electroactive materials play a vital role in the determination of specific capacitance values. The above-mentioned effects shift the low frequency capacitive behavior towards more resistive values along the real axis from which ESR (equivalent series resistance) arising due to the porous nature of the electrode material could be obtained at the frequency of 1 kHz. In the present study, the ESR value is higher due to the additional EDR (equivalent distributed resistance) arising from the resistance offered by the diffusion of ions through the pores, which contributes to the overall resistance value. The ESR of T61, T01 and T63 is 0.45, 0.468 and 0.486 Ω cm^{-2}. The ESR causes an ohmic IR drop, resulting in a decrease of the specific capacitance. This IR drop could be attributed to the resistance of the electrolytes and the inner resistance of ion diffusion in the carbon micropores.

In spite of the higher resistance and lower specific capacitance values, the carbon electrode of T63 has a fast response time: for T63, T01 and T61 this was 1.89, 2.33 and 2.57 s. This also means that T61 is more accessible than others for the pores. An interesting point concerns the slope of the plot below the knee frequency. This part of the spectrum is related to electrolyte penetration into the porous structure of the electrode. The increase of the $(\Delta Z'')/(\Delta Z')$ slope shows an improvement of the electrolyte penetration into the electrode. Seen from Fig. 6, the slope follows the sequence: T61 > T01 > T63, implying that T61 has a better penetration of electrolyte ions into the electrode. This also could be seen from the fact that the pore diameter of T63 is smaller.

Several papers [27–30] show that with decreasing frequency the current penetrates deeper into the pore, making it possible to obtain information on the pore shape from impedance measurements.

The frequency dispersion could be seen in Fig. 6, where the low frequency impedance behavior is shifted from the theoretical vertical line.

Fig. 7 shows the relationship between the total impedance and the frequency. At low frequency, the resistive and the capacitive behavior could be seen at bottom of pores, since the electrolyte ions then begin to reach deep into the pores. It could be shown from Fig. 7 that the total impedance of T63 is higher at low frequency. In Table 1, the pore diameter decreases as the characteristic energy increases. The carbon electrode T63 could be less accessible than T61 owing to the pore diameter even if the surface area of T63 is high. The small diameter micropore may not be accessible to the electrolyte solution; thus, the surface area of those non-accessible micropores will not contribute to the total double layer capacitance of the material. The pore diameter is possibly the measure of the penetrability of the electrolyte ions.

Hitz et al. [31] showed the influence of pore geometry (pear-shape, spherical and two-spheres) on the impedance spectra. With increasing f', the opening of the pores increase and the total impedance decreases, but there is also a change in general shape of complex plane plots. This means that with increases in fraction f' the high frequency feature becomes flatter and more linear, becoming increasingly similar to that of cylindrical pores. Decreasing f' shifts the low frequency capacitive behavior towards more resistive values along the real axis. This also should increase the total impedance.

In Fig. 7, the total impedance of T63 is higher at low frequency, which indicates a higher internal resistance. All of the pores of T63 should be difficult to be accessed electrochemically; that is, a lower resistance is associated with better electrolyte pore accessibility.

Fig. 8 shows a specific capacitance vs. frequency plot obtained from impedance spectroscopy. From these plots, it can be seen that all the samples exhibit a similar frequency dependence, where the capacitances decrease noticeably at high

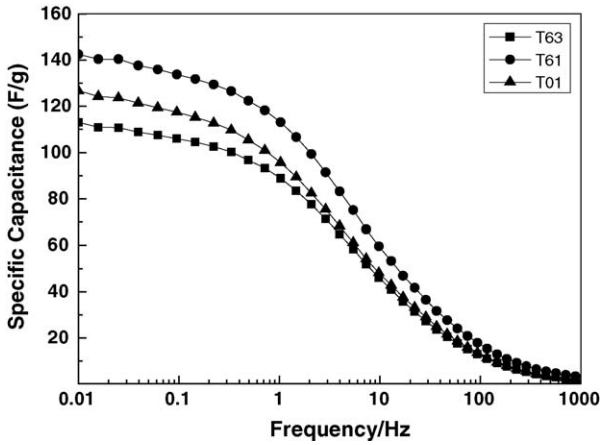

Fig. 8. Specific capacitance vs. frequency plot obtained from impedance spectroscopy.

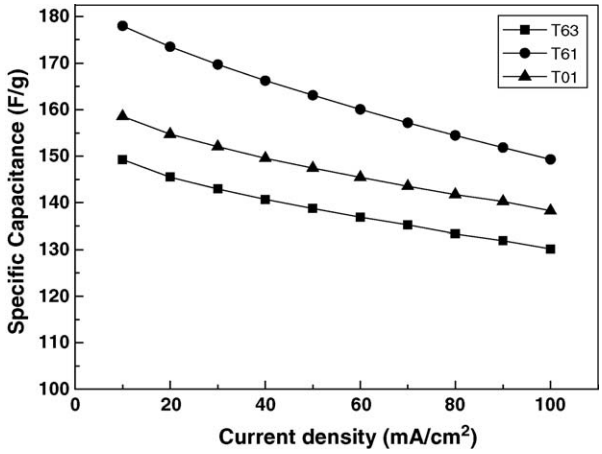

Fig. 9. Specific capacitance per unit weight of the samples as a function of the applied voltage.

frequency–a typical charging characteristic of porous electrodes. At lower frequency, the impedance plots approach a vertical line.

T61 shows a better capacitive behavior at low frequency. The pores of T61 could be electrochemically accessed rather quickly due to the larger pore diameter. The specific capacitance (C) is calculated from the imaginary part of the complex impedance according to

$$C = \frac{-1}{2\pi f Z''}$$

where f is the applied frequency; Z'' is the imaginary part of impedance.

The specific capacitance was calculated to be 142 Fg^{-1} for the carbon electrode of T61, which is higher in value than the carbon electrode of T01 (126 Fg^{-1}) and T63 (113 Fg^{-1}). The higher specific capacitance of T61 is due to the small internal resistance as shown in Fig. 7.

The time constant was calculated from the product of the capacitance and ESR (at 1 kHz) of all carbon electrodes. The time constant is the measure of how fast the pores of the electrode can be electrochemically accessed, at which time the pore walls could participate in double layer charging/discharging. The time constant of T61 is 0.33 s, for T01 it is 0.35 s and for T63 it is 0.46 s. T61 exhibited a small time constant during the penetration of electrolyte ions into the pores.

Fig. 9 shows the relationship between current density and specific capacitance by means of the 64-channel Maccor battery tester after the carbon electrode was held at a constant voltage (0.9 V) for 10 min. As shown in Fig. 9, the specific capacitance decreases gradually with increasing discharge current density at a large discharge current density that leads to a small specific capacitance.

The specific capacitance of T61 decreases more or less rapidly compared to that of T01 and T63 as current density increases. This better frequency behavior could be due to the slightly larger pore diameter of the carbon electrode, which favors a better efficiency of ions accessing the active surface.

4. Conclusion

We have studied electrochemical capacitors containing microporous PAN–ACFs as electrode materials.

The increase of specific surface area increased the micropore volume of PAN–ACF, yet decreased the micropore diameter. During the stabilization of the polyacrylonitrile fiber, tension caused a decrease of the surface area due to uncyclized regions of the fiber. The surface area of T01 was larger than that of T61.

The specific capacitance of T61 was larger than that of T01 and T63 even though the surface area of T61 was smaller. This was probably due to the larger pore diameter in spite of a pore size distribution that was narrow. The carbon electrode T63 could be less accessible for electrolyte ions than T61 owing to a small pore diameter.

Acknowledgement

This work was supported by the Core Technology Development Program of the Ministry of Commerce, Industry and Energy (MOCIE) in Korea. We are grateful for financial support.

References

[1] C.H. Kim, S.I. Pyun, J.H. Kim, Electrochim. Acta 48 (2003) 3455–3463.
[2] T. Osaka, X. Lu, M. Nojima, T. Momma, J. Electrochem. Soc. 146 (1999) 1724–1729.
[3] S.M. Lipka, Aerospace Electron. Syst. Mag. IEEE 12 (1997) 27–30.
[4] H. Nakagawa, A. Shudo, K. Miura, J. Electrochem. Soc. 147 (2000) 38–42.
[5] O. Barbieri, M. Hahn, A. Herzog, R. Kötz, Carbon 43 (2005) 1303–1310.
[6] T.C. Weng, H. Teng, J. Electrochem. Soc. 148 (2001) A368–A373.
[7] D. Qu, H. Shi, J. Power Sources 74 (1998) 99–107.
[8] G. Salitra, A. Soffer, L. Eliad, Y. Cohen, D. Aurbach, J. Electrochem. Soc. 147 (2000) 2486–2493.
[9] K. Kierzek, E. Frackowiak, G. Lota, G. Gryglewicz, J. Machnikowski, Electrochim. Acta 49 (2004) 515–523.
[10] H. Shi, Electrochim. Acta 41 (1996) 1633–1639.
[11] S.W. Hwang, S.H. Hyun, J. Non-Cryst. Solids 347 (2004) 238–245.
[12] K. Babel, K. Jurewicz, J. Phys. Chem. Solids 65 (2004) 275–280.
[13] A. Yoshida, I. Tanahashi, A. Nishino, Carbon 28 (1990) 611–615.
[14] S. Minoura, S. Nakatani, T. Morimoto, H. Oda, Tanso 210 (2003) 211–216.

[15] C.T. Hsieh, H. Teng, Carbon 40 (2002) 667–674.
[16] B. Kastening, M. Heins, Electrochim. Acta 50 (2005) 2487–2498.
[17] A. Jänes, L. Permann, M. Arulepp, E. Lust, J. Electroanal. Chem. 569 (2004) 257–269.
[18] M. Eikerling, A.A. Kornyshev, E. Lust, J. Electrochem. Soc. 152 (2005) E24–E33.
[19] A. Soffer, M. Folman, J. Electroanal. Chem. 38 (1972) 25–43.
[20] S.J. Gregg, K.S.W. Sing, Adsorption, Surface Area and Porosity, 2nd ed., Academic Press, London, 1982, Chapter 4.
[21] J.B. Donnet, T.K. Wang, S. Rebouillat, J.C.M. Peng, Carbon Finers, Marcel Dekker, New York, 1998, pp. 1–85.
[22] H.F. Stoeckli, L. Ballerini, S. De Bernardini, Carbon 27 (1989) 501–502.
[23] P. Ehrburger, N. Pusset, P. Dziedzinl, Carbon 30 (1992) 1105–1109.
[24] H.F. Stoeckli, Carbon 28 (1990) 1–6.
[25] S.H. Yoon, S.G. Lim, Y. Song, Y. Ota, W. Qiao, A. Tanaka, I. Mochida, Carbon 42 (2004) 1723–1729.
[26] N. Yoshizawa, K. Maruyama, Y. Yamada, E. Ishikawa, M. Kobayashi, Y. Toda, M. Shiraishi, Fuel 81 (2002) 1717–1722.
[27] R. De Levie, in: P. Delahay (Ed.), Advances in Elctrochemistry and Electrochemical Engineering, vol. 6, 1967, p. 329.
[28] K. Eloot, F. Debuyck, M. Moors, A.P.V. Peteghem, J. Appl. Electrochem. 25 (1995) 326–333.
[29] H. Keiser, K.D. Beccu, M.A. Gutjahr, Electrochim. Acta 21 (1976) 539.
[30] H.K. Song, Y.H. Jung, K.H. Lee, L.H. Dao, Electrochim. Acta 44 (1999) 3513–3519.
[31] C. Hitz, A. Lasia, J. Electroanal. Chem. 500 (2001) 213–222.